

INVESTIGATING ANOMALOUS PHOTOCHEMISTRY IN THE INNER WIND OF IRC+10216 THROUGH ALMA OBSERVATIONS OF HC₃N

Mark A. Siebert¹

Anthony J. Remijan²

¹Department of Astronomy, University of Virginia, Charlottesville, VA 22904, USA

²National Radio Astronomy Observatory, Charlottesville, VA 22903, USA

April 8, 2022

Abstract

In recent years, many questions have arisen regarding the chemistry of photochemical products in the winds of evolved stars. To address them, we used archival ALMA observations to map rotational transitions of cyanoacetylene (HC₃N) toward the inner envelope ($< 8''$) of the carbon star IRC+10216. The observed lines include the $J = 38 - 37$, $J = 30 - 29$, and $J = 28 - 27$ transitions of HC₃N. In contrast to previous observations of cyanopolynes in the same source, the maps of these molecular lines show spatially coincident, compact morphologies comprising arcs and loops, with significant enhancement in dense clumps at an angular distance of 350 AU from the central AGB star. We compared non-LTE radiative transfer models with the observed brightness distributions, and derive a fractional abundance of 10^{-8} for HC₃N at the radii probed by these lines. Considering the known gas phase formation mechanisms of these molecules, these results are consistent with enhanced photochemistry occurring in warm regions of this circumstellar envelope. Using these observations accompanied by the results of

a specialized photochemical model, we find evidence that the enhanced HC₃N abundances in the inner wind are due to a binary companion supplying UV photons to this region.

1 Introduction

Evolved stars have long been upheld as the major sites of chemical enrichment in the Universe. In the case of massive stars, this occurs in Type II supernovae that yield elements up to iron (fused in the star) and additional heavier elements through energetic r-process nuclear reactions (during the supernova). As for the more typical low-to-intermediate mass stars (< 10 solar masses) which are not large enough to fuse elements up to iron, their enrichment of the interstellar medium (ISM) occurs over a longer period of time (about 1 million years), well after they have evolved off the main sequence and reached the end of the what is known as the asymptotic giant branch (AGB). Thermally pulsing AGB stars have a complex structure comprising an inert carbon/oxygen core, a periodically igniting helium shell, a hydrogen burning shell, and a convective enve-

lope that extends out to the stellar photosphere.

In a process that is thought to be aided by stellar pulsations, material in the 2-10 stellar radii region undergoes high temperature reactions to form gas phase molecules, some of which condense and coagulate to form the seeds of silicate/carbonaceous dust grains. Radiation pressure then accelerates these grains over the local escape velocity and they are then pushed out into the interstellar medium along with gas phase material which is coupled to the dust through collisions. The result is significant mass-loss (on the order of $10^{-8} - 10^{-4}$ solar masses per year) in a large-scale wind of gas and dust that extends out to thousands of stellar radii, an object commonly known as a circumstellar envelope (CSE). These environments are well-known for their rich molecular chemistry, which can be studied using radio and submillimeter wavelength telescopes. Characterizing this chemistry is crucial to understanding the processing of stellar material as it is reintroduced into the ISM.

The general understanding of how chemistry proceeds in CSEs assumes precursor molecules (e.g. CO, HCN, SiO) form out of gas phase thermochemical equilibrium in the hot, dense inner envelope. Once they reach the outer regions where there is more ultraviolet light from interstellar radiation, these species then undergo photochemistry to form exotic product molecules (e.g. HC_5N , SiN, MgNC) (Ziurys 2006). However, recent leaps in observational capability have revealed that this picture may be much more complicated than previously thought. Agúndez et al. (2015) and Quintana-Lacaci et al. (2017) discovered that CH_3CN and NaCN are present in the inner wind ($< 5''$) of the

carbon star IRC+10216, despite their only known formation routes involving photochemistry.

One molecule that is expected to undergo a related chemistry to the two above is cyanoacetylene (HC_3N). This species and its longer cyanopolyynes counterparts were studied with ALMA by Agúndez et al. (2017), where it was seen emitting at a radius of $\sim 10''$. Although this is where HC_3N is expected to form based on photochemical models of this CSE, it is important to consider that these observations targeted low-energy rotational transitions which naturally trace lower temperature regions. In order to gain a more complete view of this molecule in the envelope of IRC+10216, and to contextualize the peculiar results of the other species discussed above, it is imperative to image more lines of HC_3N involving higher energy states that are populated in warmer regions.

To this end, we used archival ALMA observations to map the $J = 38 - 37$, $J = 30 - 29$, and $J = 28 - 27$ transitions of HC_3N toward IRC+10216. Using these observations combined with non-LTE radiative transfer models, we quantify the abundance of cyanoacetylene in the inner regions of IRC+10216 and discuss how they affect our understanding of photochemical processing in this stellar outflow.

2 Observations and reduction

We utilize observations from three publicly available archival ALMA projects to map transitions of HC_3N . Project 2016.1.00251.S provides a Band 7 spectral scan between 330 and 346 GHz using the 12m array (executed in March 2018). The

array configuration offers an angular resolution of $\sim 0''.8$ and a maximum recoverable scale of $8''$. These observations were used to produce the map of the $J = 38 - 37$ line at 345 609.0 MHz with a brightness sensitivity of 1.9 mJy/beam. This project also covers the $J = 3 - 2$ transition of ^{13}CO which was used to obtain the overall density structure of the envelope.

Project 2019.1.00507.S provides several spectral scans of IRC+10216 at Band 6 between 250 and 270 GHz using a variety of configurations for both the 12m and compact 7m arrays. Visibility data from four separate executions were combined to create a measurement set with an effective angular resolution of $\sim 0''.3$ and a maximum recoverable scale of $30''$. These observations were used to produce the map of the $J = 28 - 27$ line of HC_3N at 254 699.5 MHz with a sensitivity of 1.8 mJy/beam.

Project 2011.0.00229.S also includes Cycle 0 spectra of IRC+10216 at Band 6 using the 12m array. The array configuration offers an angular resolution of $\sim 0''.6$ and a maximum recoverable scale of $5.3''$. These observations were used to produce the map of the $J = 30 - 29$ line at 272 884.7 MHz at a sensitivity of 6.7 mJy/beam.

All data were calibrated using CASA's standard calibration pipeline. Visibilities were transformed to a velocity resolution of 0.5 km s^{-1} and deconvolution was performed using the `tclean` CASA task with briggs weighting.

3 Results

3.1 Emission Maps

Maps of the studied HC_3N lines are shown in Figure 1. All images represent emission averaged 0.75 km s^{-1} about the sys-

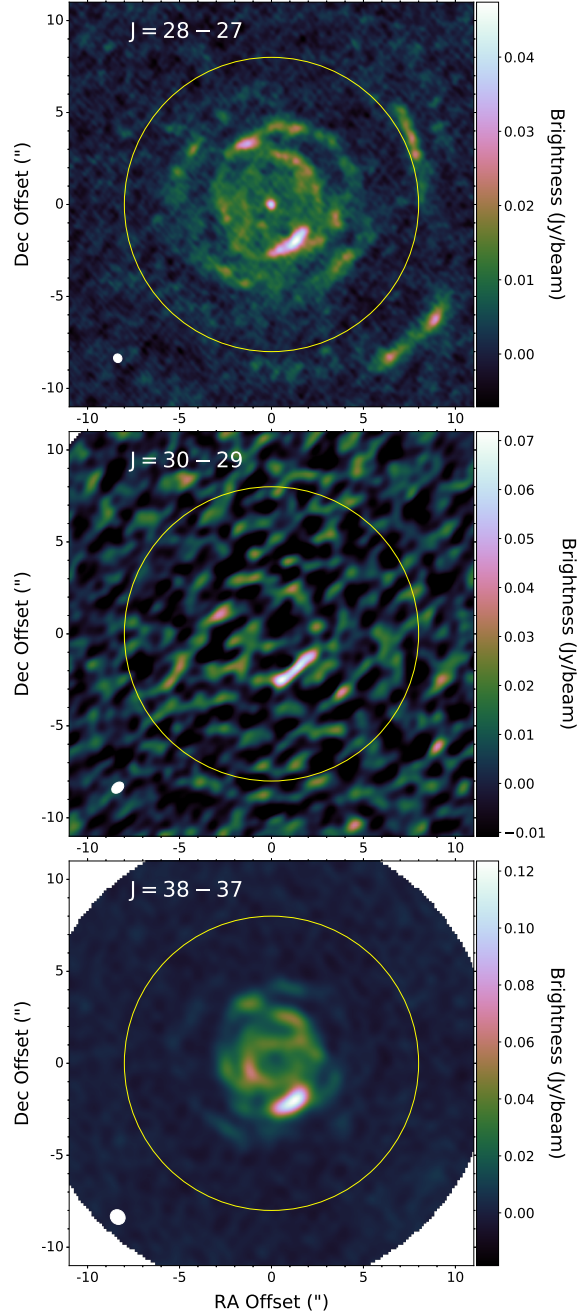


Figure 1: Emission maps of three HC_3N lines toward IRC+10216 from separate archival ALMA observations. The yellow circle denotes a radius of $7.5''$. The synthesized beam is shown in the bottom-left corner of each panel.

temic velocity of IRC+10216 ($V_{sys} = -26.5 \text{ km s}^{-1}$). These maps show primary morphologies centered on the position of the AGB star extending out to $5''$. This represents the most compact emission of a cyanopolyne molecule that has been observed toward an AGB star.

The distribution of the $J = 28 - 27$ transition shows an extended component reaching $r \sim 3''$ surrounded by density-enhanced arcs. The majority of this emission is entirely separate from that observed in the $J = 10 - 9$ line by Agúndez et al. (2017), with the notable exception of a bright clump to the SW at a radius of $10''$. In the central component, the average brightness of the line is 10 mJy/beam , with asymmetric clumps in the N and SW. Although a central peak is seen at the position of the carbon star, we expect that this is contributed from an interloping transition of an unidentified molecule, which was noted in the single-dish survey conducted by He et al. (2008). Because this transition is sufficiently far away in frequency, we expect that its distribution is a point source, and only contaminates the central part of this map.

The $J = 30 - 29$ line also appears in a bright clump to the SW which is spatially coincident with those seen in the other transitions. However due to the poor uv-coverage and sensitivity of these observations, very little additional emission is seen in this map. If this line has a similar extended component as seen in $J = 30 - 29$, we would expect most of this flux to be resolved out by the interferometer given its maximum recoverable scale. Due to these observational limitations, we did not include this line in our radiative transfer analysis.

Finally, the $J = 38 - 37$ line also

shows bright, spatially resolved emission that is entirely separate from the map in Agúndez et al. (2017). In contrast to $J = 28 - 27$, the distribution of this line is entirely concentrated within a radius of $4''$ and shows no central peak on the position of IRC+10216. The emission is again not azimuthally symmetric, and traces knots with an average brightness of 30 mJy/beam .

Figure 2 shows the maps of these HC_3N transitions as contours overlaid on a map of $^{13}\text{CO } J = 3 - 2$. Since ^{13}CO has constant abundance throughout circumstellar envelopes, it is useful as an indicator of the density structure of stellar outflows. With this in mind, we see that the bright arcs and knots traced by HC_3N are spatially coincident with density enhancements that are a result of non-isotropic mass-loss.

3.2 Non-LTE Radiative Transfer Modeling

Because the observed lines have large Einstein A_{ij} coefficients and consequently large critical densities, one cannot assume HC_3N is in Local Thermodynamic Equilibrium (LTE) within the regions probed by our observations, and computational radiative transfer calculations are necessary. Additionally, due to the differences between instrument configurations and the non-uniqueness of the image reconstruction process, care must be taken when directly comparing emission distributions between data sets.

To account for these, we employ a forward modeling approach consisting of simulated imaging with LIME (Brinch & Hogerheijde, 2010), and subsequent visibility sampling with `vis_sample`¹. LIME

¹https://github.com/AstroChem/vis_

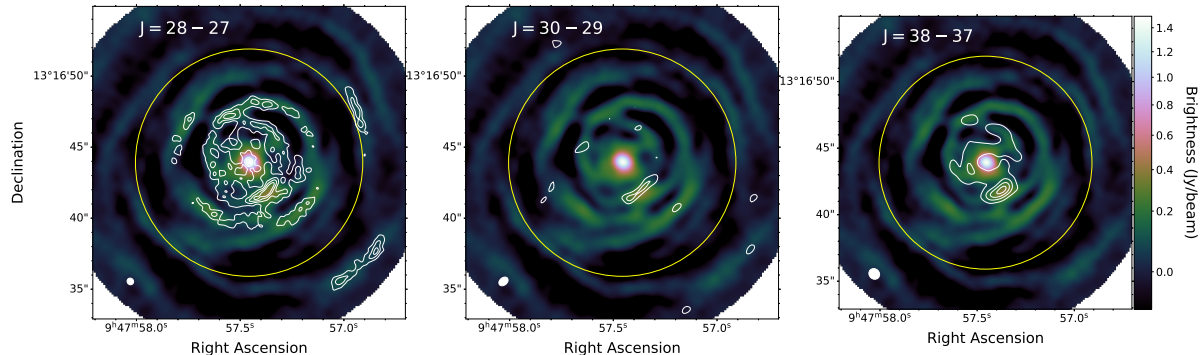


Figure 2: Map of ^{13}CO $J = 3 - 2$ emission with contours of HC_3N maps overlaid. All maps were taken at the system velocity ($V_{\text{sys}} = -26.5 \text{ km s}^{-1}$), and contours are shown at 3, 6, 9, and 12 times the rms noise of each respective image.

is a radiative transfer code used to simulate molecular excitation and radiation in astronomical environments. Given a 3D physical structure describing the density and temperature of a region along with the abundance distribution of a targeted molecule, LIME solves the populations and uses a ray-tracing algorithm to produce model image cubes of rotational lines. We then sample those images based on the uv-coverage of the observations to create model visibilities for each line. Those visibilities are then reimaged with the same parameters used to create the maps in Fig. 1.

Though LIME is capable of simulating 3D structures, we use a 1D approximation for the physical parameters of IRC+10216. Though there are clear asymmetries in the morphologies seen in Figures 1 and 2, these require computationally expensive hydrodynamical simulations to describe, and 1D approximations have been utilized successfully for chemical studies of IRC+10216 in the past (Agúndez et al., 2011).

Our model adopts the temperature and density profiles used in (Cernicharo et al.,

2011). We also use a mass-loss rate of $2.7 \times 10^{-5} M_{\odot}/\text{yr}$, which is the value obtained by Guélin et al. (2018) specific to regions within a radius of $10''$. The spectroscopic data for HC_3N was obtained from the LAMBDA database which uses the transition strengths and collisional rates from Faure et al. (2000). These rates were extrapolated to extend to include the $J = 45$ rotational level. Additionally, we take into account the affect of pumping to vibrational states via infrared photons by including the ν_5 and ν_6 transition ladders which were obtained from the HITRAN database².

To test the accuracy of our physical model and the validity of a 1D approximation, we first simulated the $J = 3 - 2$ transition of ^{13}CO . This molecule has a known constant fractional abundance of 1.3×10^{-5} with respect to H_2 (De Beck et al., 2012). Using the forward modeling approach described above, the simulated brightness profile of this transition (using only previously published parameters) is shown in the top panel of Fig. 4. From here, it is clear we are able to reconstruct

sample

²<https://hitran.org/lbl/>

the emission of this molecule, and that the visibility sampling algorithm is accurately accounting for the flux loss of the interferometer.

To apply this to HC_3N , we ran LIME for several abundance profiles. The shape of these profiles was motivated by the results of the chemical model by Agúndez et al. (2017). The resulting best fit profile is shown in Fig. 3, and its comparison with the observations is shown in the bottom two panels of Fig. 4. We find that a fractional abundance with respect to H_2 of 10^{-8} is needed to reproduce the average intensity in our maps, and that this abundance must be increasing with radius in this region to explain the distribution of the observed brightness. When compared with the results of previous chemical models, this represents a stark overabundance of at least one order of magnitude.

4 Discussion

From our observations, it is clear that HC_3N is forming more readily between distances of 10^{15} and 10^{16} cm from IRC+10216. One possible explanation for this behavior, in addition to the observed abundances of other photochemical products discussed previously, is that an embedded binary companion star could be supplying UV photons to the inner regions of this circumstellar envelope. Previous studies of IRC+10216 have concluded that it is part of a binary system (Guélin et al., 2018), and if its companion has a high enough temperature, its radiation could be enough to influence the chemistry of the envelope.

To test this hypothesis, we employed the photochemical model of Van de Sande et al. (2021), which was built to predict

molecular abundances in AGB envelopes with an internal source of UV radiation. This model was run using the same physical parameters of IRC+10216 discussed in Section 3.2. In addition, this chemical model uses a porosity formalism to describe the clumpiness of the outflow. The main components of this formalism are the clump volume filling factor (f_{vol}) which describes the fraction of the envelope that is occupied by clumps, and the clump-interclump density contrast (f_{ic}), which describes how overdense the clumps are. We ran this photochemical model for a wide range of companion scenarios.

In all models, a binary companion with surface temperature larger than 6000 K causes an increased abundance of HC_3N within a radius of 10^{16} cm relative to the companionless model. An example of this is shown in Fig. 3. While these models can reproduce the $\sim 10^{-8}$ abundance feature constrained by our observations, there is a notable difference in the shape of the profiles. In the companion models we see a much shallower, almost constant slope at inner radii, whereas the observations suggests the abundance tapers off around 10^{15} cm. This could be explained by some of the limitations and approximations of the chemical model, namely that all the companion photons are release instantaneously into the porous wind. So further investigation is needed to resolve these details.

5 Conclusions

We conducted a study of the photochemical product cyanoacetylene (HC_3N) toward the carbon star IRC+10216 using archival ALMA observations. Through rigorous simulations of the observed lines we identify a clear enhancement of this

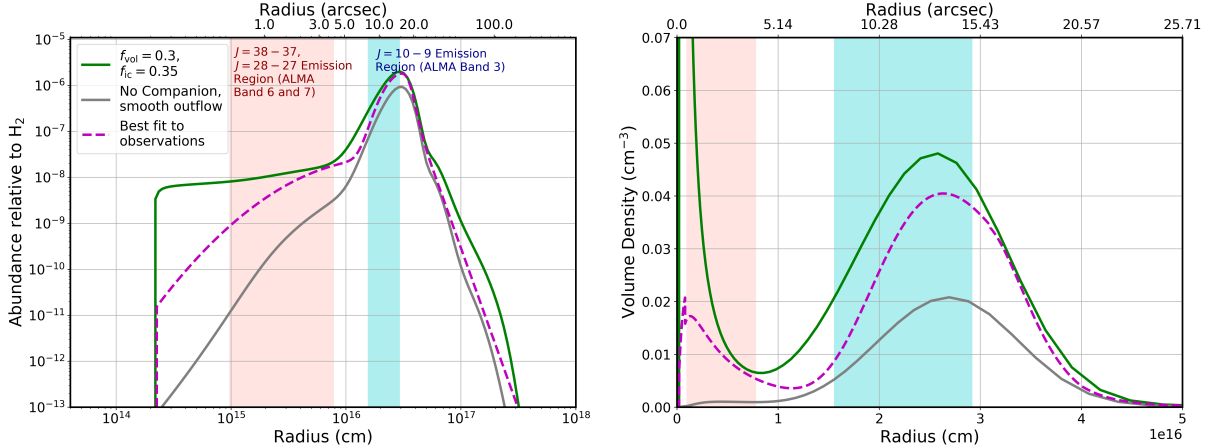


Figure 3: *Left*: Abundance profiles of the best fit model based on LIME modeling of observations (dashed), and results of the photochemical model (green and gray solid lines). Green curve is the result of a 6000 K companion at $5R_{\text{dust}}$, while the gray curve was run with no companion photons. *Right*: Volume density profiles of the same scenarios.

molecule within a radius of 5'' from the AGB star. We then compared these results with the predicted abundances of a specialized photochemistry model and find that the observations could be explained, in part, by a 6000 K stellar companion embedded near the dust formation region of IRC+10216.

The implications of this result on how we understand stellar recycling are exciting. In recent years, it has become more clear the important role binary stellar companions of AGB stars play in their mass-loss and envelope morphology (Decin et al., 2020), but this is the first direct evidence we see of a companion influencing the chemistry and processing stellar material as it is released into the ISM. Similar future astrochemical studies into IRC+10216, other binary AGB stars, and proto-planetary nebula will be instrumental in reframing how gas and dust are processed in stellar envelopes.

References

- Agúndez, M., Cernicharo, J., Quintana-Lacaci, G., et al. 2015, *ApJ*, 814, 143, doi: 10.1088/0004-637X/814/2/143
- Agúndez, M., Cernicharo, J., Waters, L. B. F. M., et al. 2011, *AA*, 533, L6, doi: 10.1051/0004-6361/201117578
- Agúndez, M., Cernicharo, J., Quintana-Lacaci, G., et al. 2017, *A&A*, 601, A4, doi: 10.1051/0004-6361/201630274
- Brinch, C., & Hogerheijde, M. R. 2010, *AA*, 523, A25, doi: 10.1051/0004-6361/201015333
- Cernicharo, J., Agúndez, M., Kahane, C., et al. 2011, *AA*, 529, L3, doi: 10.1051/0004-6361/201116717
- De Beck, E., Lombaert, R., Agúndez, M., et al. 2012, *AA*, 539, A108, doi: 10.1051/0004-6361/201117635

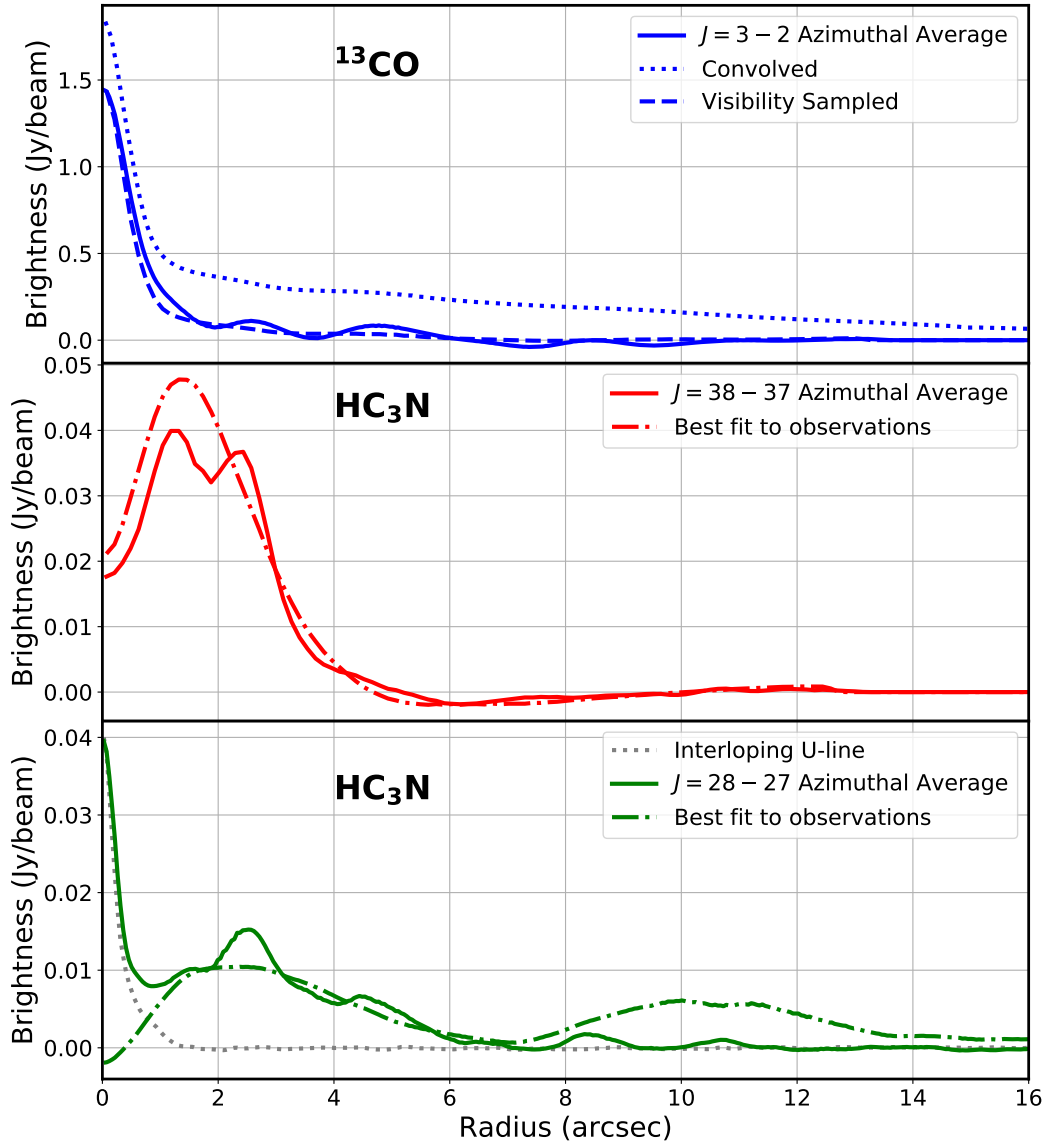


Figure 4: Azimuthal averaged brightness distributions of ^{13}CO (top), and the two HC_3N lines we model with LIME. Dash-dotted lines correspond to the visibility sampled RT models using the abundance profile shown in Fig. 3. For ^{13}CO , the visibility sampled result is shown (dashed) in reference to a plain convolution of the LIME image cube (dotted).

Decin, L., Montargès, M., Richards, A. M. S., et al. 2020, *Science*, 369, 1497, doi: 10.1126/science.abb1229

Guélin, M., Patel, N. A., Bremer, M., et al. 2018, *AA*, 610, A4, doi: 10.1051/0004-6361/201731619

He, J. H., Dinh-V-Trung, Kwok, S., et al. 2008, *ApJS*, 177, 275, doi: 10.1086/587142

Quintana-Lacaci, G., Cernicharo, J., Velilla Prieto, L., et al. 2017, *AA*, 607, L5, doi: 10.1051/0004-6361/201732015